ADVANCED FUNCTIONAL MATERIALS
www.afm-journal.de

Composition Waves in Solution-Processed Organic Films and Its Propagations from Kinetically Frozen Surface Mesophases

Jinde Yu, Zichao Shen, Wanlong Lu, Yuanwei Zhu, Yi-Xin Liu, Dieter Neher, Norbert Koch, and Guanghao Lu**

Organic thin films deposited from solution attract wide interest for next-generation (opto-)electronic and energy applications. During solvent evaporation, the phase evolution dynamics for different components at different locations are not synchronic within the incrementally concentrated liquid films, determining the final anisotropic morphology and performance. Herein, by examining tens of widely investigated optoelectronic organic films, the general existence of composition wave propagating along the surface-normal direction upon solidification is identified. The composition wave is initiated by a few nanometers thick surface mesophase kinetically forming at the foremost stage of phase transition, and afterward propagates toward the substrate during solvent evaporation. The composition waves exhibit well-defined wave properties, including spatial wavelength, period, amplitude, and propagation velocity. These wave properties are closely correlated with the evaporation rate and the diffusion rate of organic molecules, which determines the dynamically varied local composition gradient along the surface-normal direction. Such composition waves are commonly found for more than 80% of randomly examined solution-processed thin films for high-performance organic electronic devices including photovoltaic cells and field-effect transistors.

1. Introduction

The possibility to deposit organic semiconductor and conductor thin films from solution substantially expands the potential of next-generation electronic, optoelectronic, and energy application.[1–3] Solution-processed films, particularly when cast from solutions containing more than one compound, are often anisotropic, featuring laterally and vertically varying properties.[4–7] During solution deposition, the incremental evaporation of solvent leads to dynamic local changes of local solute concentration and gradually increased viscosity, causing that the solute concentration varies with both time and vertical position during the drying process, which can also result in vertically varying properties of the resulting dry film. For multicomponent solutions, the phase evolution of the different components during the drying process depends on their solubility and the molecular diffusion rate. Since these can differ, one component might undergo a phase transition in solution before the other at a given overall solute concentration. However, the phase evolution dynamics of organic films in terms of space (vertical position between substrate and surface, also termed "film-depth" or "surface-normal") and time during the drying process, are challenging to be captured, because state-of-the-art characterization approaches are not sufficient for

J. Yu, Z. Shen, W. Lu, Y. Zhu, G. Lu
State Key Laboratory of Electrical Insulation and Power Equipment, and Frontier Institute of Science and Technology
Xi'an Jiaotong University
Xi'an 710049, China
E-mail: guanghao.lu@mail.xjtu.edu.cn

Y.-X. Liu
State Key Laboratory of Molecular Engineering of Polymers
Department of Macromolecular Science
Fudan University
Shanghai 200438, China
E-mail: lyx@fudan.edu.cn

D. Neher
Institut für Physik und Astronomie
Universität Potsdam
14476 Potsdam, Germany

N. Koch
Institut für Physik & IRIS Adlershof
Humboldt-Universität zu Berlin
12489 Berlin, Germany

N. Koch
Helmholtz-Zentrum Berlin für Materialien und Energie GmbH
12489 Berlin, Germany

The ORCID identification number(s) for the author(s) of this article can be found under https://doi.org/10.1002/adfm.202302089

DOI: 10.1002/adfm.202302089

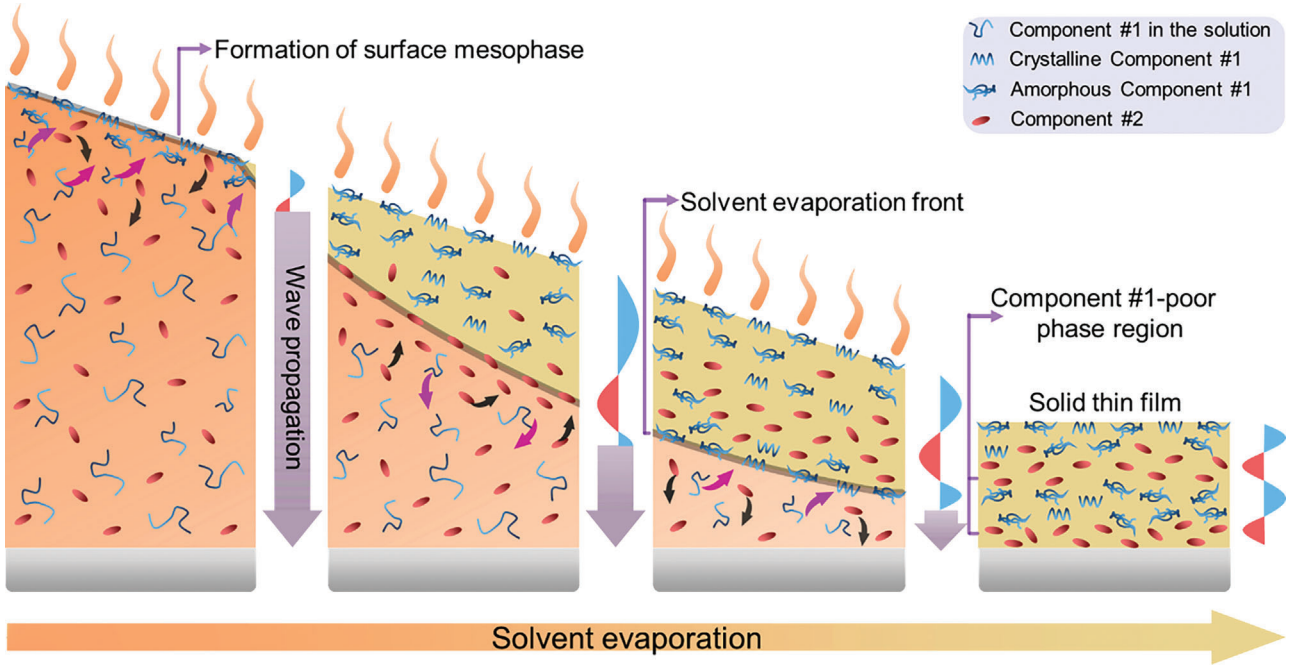

Figure 1. The schematic diagram of wave-like propagation of phase evolution dynamics during solvent evaporation. During the rapid solvent evaporation, the concentration of solution surface quickly increases. A surface mesophase (severe surface pre–aggregation) of Component #1 with relatively poor solubility and/or limited diffusion rate could firstly form on the upper surface of the blend solution, and subsequently the compositional fluctuation would grow in amplitude near the surface mesophase for Component #1. Afterward, this periodical phase segregation propagates toward the substrate, resembling a wave-like propagation along surface-normal direction. Finally, a vertical composition wave forms, composed by Component #1-rich/poor phase regions in organic thin film. The red and blue sinusoidal blocks on the right margin represent the phases of the wave, while the "phase" (positive or negative) of the wave function corresponds to the composition "phase" (Component #1 or Component #2). The light black and light red arrows in each blend solution indicate the molecule diffusion directions of the two components in the solvent evaporation front.

providing the desired insight with millisecond and nanometer resolution.

The thin-film solidification process during solvent evaporation has been investigated with in-situ and ex-situ measurements, such as optical absorption and reflectivity spectroscopy[8–10] and X-ray scattering,[11,12] to study the nucleation, growth, crystallization as well as molecular aggregation,[13–15] which provided some understanding of the relevant phase transition mechanisms. In particular, these investigations found that the morphology optimization is basically governed by thermodynamic molecular interactions and careful materials matching must be pursued for optoelectronic device performance improvement.[16,17] Such explorations commonly include phase diagrams to understand the phase behavior of multicomponent systems.[18–21] However, solution-deposited organic thin films are commonly processed within comparably short time, with accordingly rapid solvent evaporation, so that the nonequilibrium kinetics of film solidification largely determine the resulting film morphology. Consequently, investigation and manipulation of the phase evolution dynamics at different film-depth and time scales are attracting increasing interest in the pertinent research community.

Along these lines, the nonhomogeneity of organic blend films has been intensively studied, and nonlinear composition profile[22] along the surface-normal direction have been reported. However, the underlying formation process of this nonlinear distribution is still not resolved, i.e., the propagation of phase fluctuation was not yet reported. Likewise, eventual propagating wave properties of the fluctuations, such as period, frequency, and velocity, as well as wave initiation and propagation direction remain elusive.

In this present study, a number of two-component systems are chosen for investigation of the phase evolution dynamics by a combination of time- and space-resolved optical spectroscopies. A composition wave propagating along the surface-normal direction is reported here. The schematic diagram in **Figure 1** demonstrates this kinetics process and the propagation of the composition wave in a two-component system. In the beginning, the top surface of solution quickly concentrates during solvent evaporation, thus a surface mesophase for Component #1 with a few nanometers thickness forms as a result of the increased solution viscosity and limited molecular diffusion, which initiates the propagation of such a composition wave along the surface-normal direction. Subsequently, the compositional fluctuation would grow in amplitude near the surface mesophase for Component #1. Afterward, this periodical phase segregation propagates toward the substrate during further solvent evaporation, while the spatial wavelength, period, amplitude, and propagation velocity are correlated with the solvent evaporation rate and diffusion rate of different organic molecules. Finally, a vertical composition wave forms, composed by Component #1-rich/poor phase regions. For clarity, the phase evolution here tentatively refers to the development of vertical composition gradients or waves, while the phase may be not a well-defined pure matter. It also needs to be noted that such surface mesophase (severe

surface pre–aggregation) appeared in the air-solvent interface is induced by the competition between the of solvents evaporation and components diffusion, which is quite different from the pre–aggregation formed by π–π intermolecular interaction in the bulk solution. Computational simulations do corroborate the wave-like propagation of phase evolution dynamics induced by the formation of a surface mesophase. By examining a variety of such solution-processed thin films reported in the literature for organic photovoltaics (OPV), it is also found that such wave-like periodical phase segregation is commonly found in many high-performance heterogeneous systems. In addition, the phase evolution of the model-conjugated polymer regioregular poly(3-hexylthiophene) (rr-P3HT) in blend with amorphous regiorandom P3HT (rra-P3HT) shows that the composition wave is even present in neat semicrystalline polymer films.

2. Results

2.1. Formation and Evolution of Surface Mesophases in J71:ITTC Solution During Solvent Evaporation

Although vertical phase segregation is a common phenomenon in organic multicomponent systems, often playing a crucial role in device performance, the formation mechanism of vertical phase segregation during solvent evaporation is yet unresolved. Here, time-dependent reflection spectroscopy is applied to explore the dynamic phase evolution of a two-component system that is of relevance for surface mesophase and diffusion rate. To unravel the phase evolution and precipitation sequence of the two solutes, J71[23] and ITTC[24] (molecular structure is shown in **Figure 2**a) in chlorobenzene (CB) solution, we probe the reflected light of the blend during the spin-coating process at room temperature. Figure 2b shows the real-time evolution of optical reflection spectra for J71:ITTC solution just right after deposition on a quartz substrate, where the light black arrow indicates the overall timeline. All reflection spectra cover the UV–vis region, ranging from 300 to 1100 nm. In order to obtain a better view of the spectral evolution, the time-dependent reflection spectra are divided into three parts according to the peak shape of the spectra as depicted in Figure 2d. During the first stage of drying (0–1.6 s, black lines), there is a deep well-like feature in the reflection spectra in Figure 2b, located in the wavelength range of 400 to 750 nm. In fact, this region comprises two peaks at 536 and 586 nm (0 s) that can be seen upon rescaling in Figure 2d. This initial stage corresponds to a thick liquid film (≈10 µm). Afterward, the excess blend solution on the quartz substrate is removed during spinning the sample (mounted on a spin coater), and the peak shape of the reflection spectra undergoes notable changes. Three different peaks (550, 600, and 649 nm, at 1.7 s) appear owing to the sharp decrease in liquid film thickness. During this stage (1.7–5.2 s, blue lines), the solvent of thin liquid film evaporates quickly and a gradual increase in the intensity of the reflection peaks (400–750 nm) is observed. During the third stage (5.3–40 s, red lines), a characteristic reflection peak of the acceptor appears at 770 nm, which is attributed to minuscule solvent content in organic blend film. In addition, the intensity of three peaks at 550, 600, and 649 nm (5.2 s) rises to a maximum in a few seconds. As for J71, its peaks gradually blue-shifts to 541 and 590 nm (40 s), which are the intrinsic reflection peaks of a J71 dry thin film. In the case of ITTC, the shoulder peak at 649 nm (5.2 s) finally moves to 660 nm (40 s) and the intrinsic reflection peak at 770 nm appears. During the first two stages, the reflection peaks at 770 nm are absent due to the good solubility of ITTC in CB and the high reflectivity of solvent above 750 nm. Unexpectedly, it is found that the reflection peak of J71 (ranging from 470 to 630 nm) exhibits little differences between the thick liquid film and the dry film, suggesting that the J71 polymer segregates at the surface of the liquid film and thus forms a distinct surface mesophase during solvent evaporation. Moreover, no reflection shoulder-peak of ITTC is observed around 660 nm (0–1.6 s), which indicates that ITTC does not segregate at the thick liquid film surface. At the intersection of the second and the third stage (5.2 s, blue line and 5.3 s, red line), it is also seen that the precipitation of the J71 polymer takes precedence over that of the ITTC small molecules on account of strong reflection double peak of J71 and very weak reflection shoulder peak of ITTC. The reflected light path in the thick liquid film is illustrated in Figure 2a. In the thick liquid film, the spectrophotometer can only capture the reflected signal from surface mesophase, and the source light incident into wet films cannot be reflected from the bottom of the sample due to the high thickness of the liquid film and the high extinction coefficient of organic semiconductors. Therefore, time-dependent reflection spectroscopy is an effective technique to monitor the formation of surface mesophases during evaporation and to distinguish a sequential order of various solutes in multicomponent systems, especially for high-efficiency nonfullerene OPV systems.[25]

To investigate the influence of a lower-boiling point solvent on the evaporation dynamics and phase segregation of the J71:ITTC blend, we choose chloroform (CF) as solvent and performed analogous time-dependent reflection spectroscopy. Figure 2c shows the variation of reflection spectra as function of time. As above, this process also contains three stages as represented in Figure 2e. The drying time for CF-based solution is shorter than 5 s compared with that of CB-based solution. It is apparent that a new peak at 655 nm arises, belonging to the ITTC shoulder peak reflection, which leads to the apparent red-shift of the J71 original main reflection peak (586 nm) to 595 nm, while no obvious change occurs for its minor peak at 536 nm (0 s, Figure 2e). Thus, the simultaneous separation of J71 and ITTC ascribable to the rapid evaporation rate is observed and a binary surface mesophase is formed in this initial stage. The dynamics for the next two stages are almost identical to that observed for CB-based solution, but on shorter time scale.

Solvents with low boiling point tend to favor the formation of surface mesophases, typically driven and governed by the evaporation rate. Consequently, it is essential to explore the surface mesophase of J71:ITTC blend solution in different solvents. In the following, three common solvents, CF, CB, and *o*-dichlorobenzene (*o*-DCB), are utilized to study the effect of solvents on the surface conditions. The resulting reflection spectra are shown in Figure 2f, which confirm that surface mesophase formation does depend on solvent type and its evaporation rate. In contrast, it is known that the intensity of J71 reflection spectra peaks (536 and 586 nm) in hot CB solution (100 °C) prevails over the CB solution at room temperature of a thick liquid film, indicating that the J71 polymer segregates more easily owning to faster evaporation rate of CB when heated. Nevertheless, the J71 reflection peaks apparently exist in the hot *o*-DCB solution and

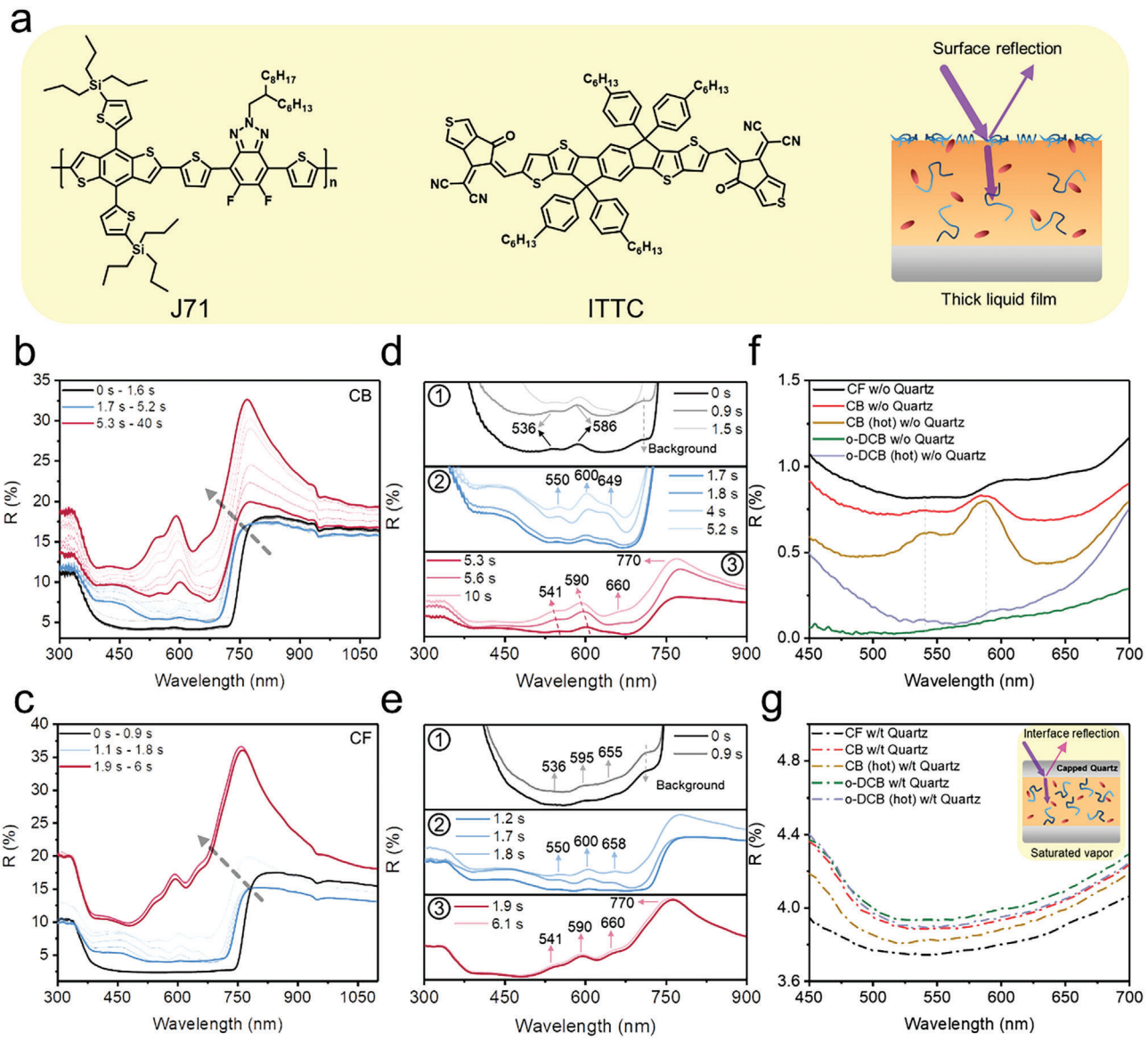

Figure 2. The formation and evolution of surface mesophase in the J71:ITTC solutions during solvent evaporation. a) The molecular structure of J71:ITTC and schematic diagram of light reflection for thick liquid films. b,c) Time-dependent reflection spectroscopy of J71:ITTC (1:1) films deposited from chlorobenzene (CB) (b) and chloroform (CF) (c) solutions, respectively. d,e) Rescaled reflection spectra as obtained from (b) and (c). The reflection features at wavelength 541 and 590 nm are characteristics of J71 mesophase. f,g) Reflection spectroscopy of J71:ITTC solution. Surface mesophase measurements in different solutions without (f) or with (g) saturated solvent vapor pressure. The inset of (g) schematically shows the saturated solvent vapor achieved by a quartz on the top surface of the solution, which prevents the solvent evaporation.

tiny signals are observed at room temperature, because *o*-DCB has a high boiling point and is less volatile than CB, and thus polymer chains have sufficient time to diffuse downward to the inner part of the solution. As for J71:ITTC in CF solution, its comparably high evaporation rate leads to simultaneous separation of J71 and ITTC. However, J71:ITTC is actually endowed with good solubility in CF, better than in CB or *o*-DCB solvents, thus with weak reflection peaks intensity. This further demonstrates that the appearance of reflection peaks for thick liquid film is caused by surface mesophases. A kinetic variation of solvent evaporation was realized through covering the blend solution with a quartz plate before spin-coating, so that the solvent is essentially non-volatile and no air-solvent interface exists. This procedure aims to simulate a saturated vapor pressure atmosphere for the solutes. Figure 2g presents the reflection spectra of quartz-capped solution for the different solvents. Unlike the reflection spectra in Figure 2f, all reflection peaks (particularly at 536 and 586 nm) in Figure 2g disappear, making it clear that a surface mesophase is absent in such capped solutions whether at room temperature or at elevated temperature. The inset diagram in Figure 2g shows the reflection measurements of the surface mesophase, illustrating that capped quartz on the solution compels surface mesophase to redissolve, bringing about the disappearance of the surface mesophase reflection peaks. Additionally, the dynamic

light scattering is carried out for scattering and photoluminescence measurement during the film-formation process, as shown in Figure S7 (Supporting Information). Given by the well miscibility of J71 and ITTC, the dynamic light scattering is not able to characterize subtle vertical phase separation. However, the periodical photoluminescence decline can be observed, indicating the asynchronous aggregation of J71 and ITTC in different solvents during its evaporation.

Furthermore, to validate that the formation of surface mesophases exist in several multicomponent high-efficiency OPV systems, numerous material pairs, such as FTAZ:ITIC-Th1,[26] J52:IEICO,[27] J52:ITIC,[28] PM6:IT-4Cl,[29] and PBDB-T:ITIC,[30] were investigated according to the fabrication conditions reported in the literature. All material pairs exhibit characteristic reflection peaks of surface mesophase and similar phase evolution occurs (Figure S9, Supporting Information), indicating surface mesophase formation of the polymer components in the initial thick liquid films. Film-depth-dependent light absorption spectroscopy (FLAS) of these material pairs (Figure S11, Supporting Information) further demonstrates that the top surfaces of the respective solid films are mainly dominated by the polymer compound, as a result of slower diffusion rate of polymer chains as compared with small molecules.

2.2. Variation of the Wave Properties Including Period, Velocity, and Amplitude upon Manipulating the Phase Segregation Dynamics

FLAS is hereby utilized to study the phase segregation of dry films in the vertical direction (normal to the film surface).[31,32] **Figure 3**a,b shows spectra of J71:ITTC films fabricated from CB and CF, and each spectrum is for a sublayer with a thickness of ≈7–10 nm. Apparently, these two kinds of organic thin films exhibit rather contrasting phase segregation. A periodic layered structure, such as A-B-A-B, appears in the thin film made from CB solution, while the other made from CF solution is comparably uniform without apparent layered structure. For the J71:ITTC blend film (CB), the first top line in Figure 3a is from the surface with predominant J71 polymer presence. In contrast with the J71:ITTC blend film from CF, its surface comprises both J71 and ITTC (the first top line in Figure 3b), because the rapid solvent evaporation does not allow for sufficient time for phase separation. It can be inferred that the surface compositions in Figure 3a,b vary widely by virtue of disparate surface mesophase states of the liquid films (as discussed for Figure 2b,c). Right underneath the polymer-enriched surface layer, a pronounced polymer-poor phase region with thickness around 10 nm is formed (the second and the third spectra of FLAS from top in Figure 3a,b). Further calculation upon Beer-lambert Law confirms a compositional wave along the film-depth direction in Figure 3g. In analogy to mechanical waves, such vertical composition fluctuations in organic thin films can be described in analogy. In general, a wave-like pattern along the surface-normal direction occurs twice for the repeating structural unit "J71-ITTC" ("J71" here means the sublayer at a given depth is dominated by J71, and analogously for "ITTC") in thin films deposited from CB, which can be noted as 2T per 100 nm (2T represents half the number of extreme points for J71 or ITTC curves in composition distribution profile). Thus, the period of "wave" in thin film deposited from CF is 2.5T per 100 nm. The propagation velocity of the composition waves in thin films deposited from CB and CF are about 5 and 20 nm s^{-1}, respectively (dry film thickness divided by kinetic evaporation time). In addition, the amplitude of a "wave" varies for each sublayer, and the amplitudes of top and bottom interface are larger than that of the inner film (fabricated from CB), while the amplitude of "waves" for the thin film from CF changes little overall, which demonstrates the phase segregation of the thin film from CB is more significant than that from CF. The mean amplitude of "wave" (A_m), defined as the average of the maximum and extreme values on the component ratio curve for the J71 polymer, can describe the degree of vertical phase segregation of the whole thin film. A_m is a dimensionless percentage value (no unit), because it is the percent by weight (wt%) for the donor (J71) or acceptor (ITTC). The calculation of the mean amplitude (ranging from 0 and 0.5) can be performed with:

$$A_m = \frac{\sum_{i=1}^{n} |R_i - 0.5|}{n} \quad (1)$$

Here, R_i is the component ratio of donor polymer at certain maximum and extreme value point. A_m for the thin films from CB and CF is 0.38 and 0.13, respectively, indicating that the thin films from CB exhibit a more pronounced vertical phase segregation compared with that from CF. Moreover, the degree of phase segregation for very surface layer can be represented by the surface amplitude (A_s), $A_S = |R_S - 0.5|$, R_s is the component ratio of surface layer for polymer. Thus, the values of R_s are 0.5 and 0.18 for CB and CF, respectively, meaning that the thin film from CB is completely covered by J71. Additionally, it is noted that stripes of light and dark in the grayscale image (Figure 3g) is a better way to illustrate that such periodical "wave" is indeed a composition wave, i.e., a darker gray value corresponds to higher content of J71. Actually, surface enrichment of one component[33–36] or surface-segregated monolayer[37–39] has been found in some organic blend thin films. The dominant viewpoint of this phenomenon is mostly based on the difference in surface energy.[40] Previous experiments show no clear evidence on the existence of surface separation with a top mesophase layer in such blend solutions, which is more of a conjecture from the vertical composition profiles in organic thin films. At this point, we obtain the fact of when and where the separation of surface layer appears in such organic blend solutions.

Mixed solvents or additives are the most practical way to realize miscellaneous morphological structures of organic thin films. In this study, CF/*o*-DCB-mixed solvents, with varied *o*-DCB volume percentage, are applied to tune the oscillation properties of the wave-like phase segregation. Figure 3c–f shows the FLAS of four thin films fabricated from several mixed solvents, where the volume contents of *o*-DCB in CF range from 1% to 8%. The FLAS in Figure 3c,d exhibits little difference from that in Figure 3b and a, respectively. Further calculations indicate that they indeed have similar composition distribution curves (Figure 3g,h). When the volume fraction of *o*-DCB in CF reaches 5% or more, Figure 3e,f presents quite distinctive FLAS and vertical phase separation, which is akin to a bilayer thin film with J71 mainly in the upper layer and ITTC in the bottom layer, confirmed by the results in Figure 3i. Overall, the periods of "waves" from mixed solvents are

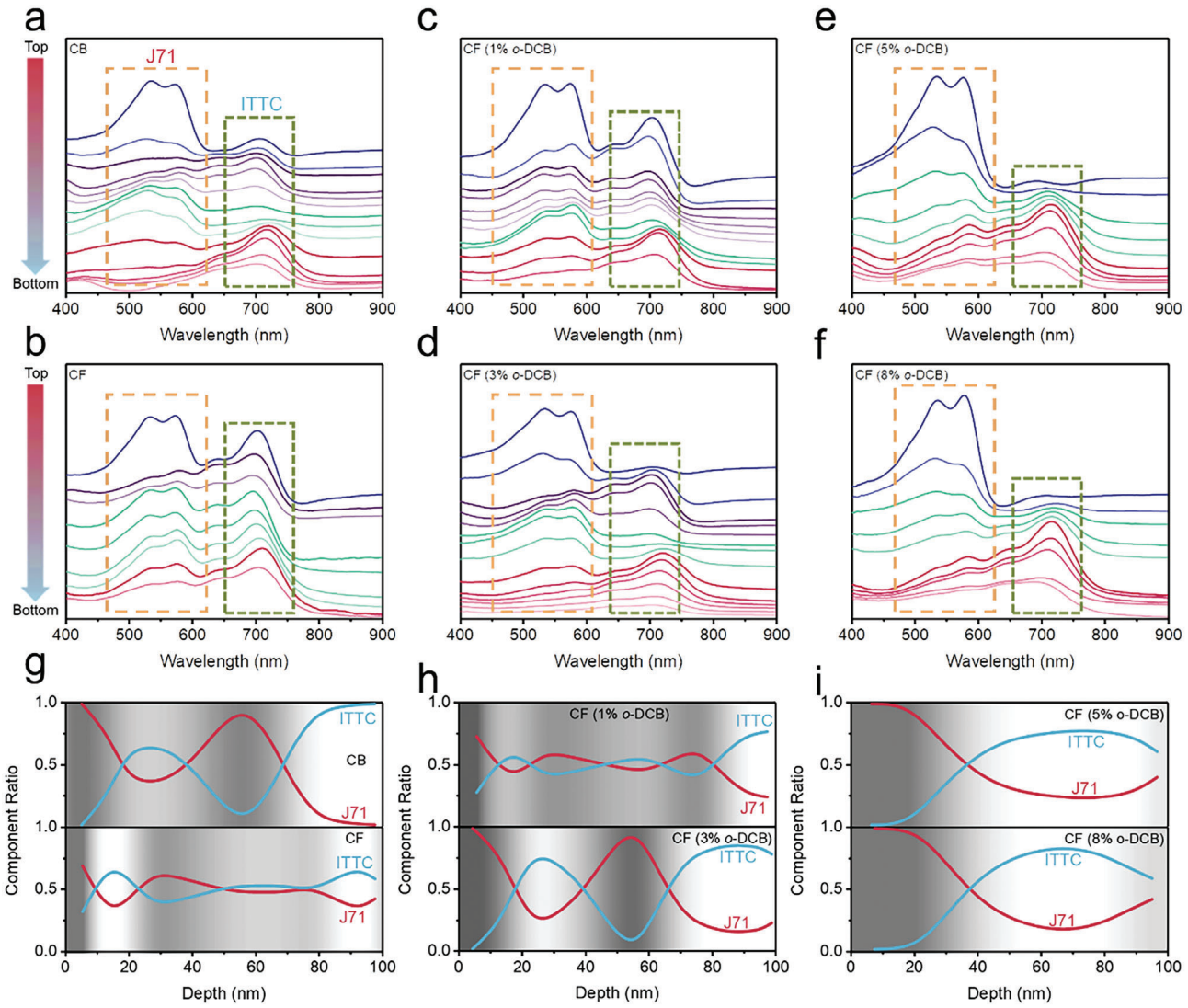

Figure 3. Variation of the wave properties including period, velocity, and amplitude upon manipulating the phase segregation dynamics. a–f) Film-depth-dependent light absorption spectroscopy (FLAS) of J71:ITTC films deposited from different solvents. The spectra are vertically arranged along the surface-normal direction, and the dashed boxes show the absorption peaks of J71 and ITTC. Each spectrum represents a light absorption characteristic of a sublayer with thickness around 10 nm. g–i) Composition distribution profiles at different film-depths as numerically extracted from (a–f). The grayscale background is guided to illustrate that such a wave-like phase segregation scenario represents a composition wave, where the gray value represents the wave phase, and higher gray corresponds to higher content of J71.

3T, 2T, 1T, and 1T per 100 nm, respectively. A_m is 0.13, 0.38, 0.39, and 0.42, and A_s is 0.22, 0.5, 0.5, and 0.5, respectively. Regardless of A_m or A_s, the value of amplitudes and phase separations tend to become larger with increasing *o*-DCB content, indicating the amount of high boiling-point solvent contributes to tune the periodicity of such composition waves in organic thin film. The corresponding grayscale images in Figure 3h,i also show the periodic structure of composition waves. The intense amplitude directly induces the formation of large-scale phase separation during solvent evaporation. In one word, the rate of solvent evaporation determines the properties of composition wave, such as spatial wavelength, period, amplitude, and propagation velocity, resulting in different vertical phase separation of active layer.

2.3. Computational Simulation of Composition Wave Evolution in J71:ITTC Solution During Solvent Evaporation

Previous study has shown that the formation of a skin layer (surface mesophase)[41] is an essential competition between the evaporation of the solvents and the diffusion of the polymer component in the solution. A gel-like surface mesophase is formed when the evaporation is much faster than the diffusion. Here, phase-field simulations adopt similar approach as the formulation to describe the evolution of composition waves during the solidification process of our organic blend films. The volume fractions of components A and B, $\phi_A(r)$ and $\phi_B(r)$, follow the equations during the evaporation of solvents.

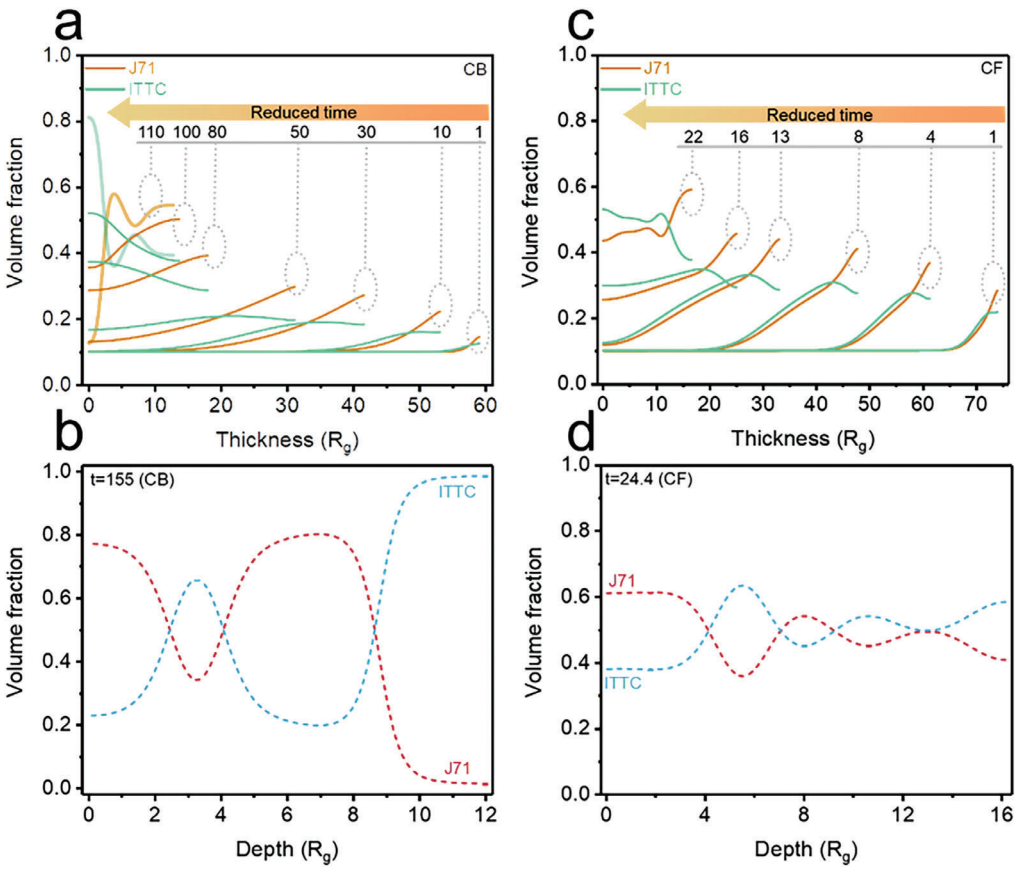

Figure 4. Computational simulation of composition wave evolution during solvent evaporation. a,b) Numerically simulated phase segregation dynamics evolution of J71:ITTC in CB solution (a) and in its corresponding dry film (b). c,d) Numerically simulated phase evolution dynamics of J71:ITTC during the solvent CF evaporation (c), and film-depth-dependent composition distribution in its corresponding dry film (d). The orange arrows in (a) and (c) indicate the time axis for the solvent evaporation. The time axis is in arbitrary units.

$$\frac{\partial \phi_A}{\partial t} = D_A \nabla \left[\phi_A \nabla \tilde{\mu}_A\right] \quad (2)$$

$$\frac{\partial \phi_B}{\partial t} = D_B \nabla \left[\phi_B \nabla \tilde{\mu}_B\right] \quad (3)$$

where $\tilde{\mu}_A$ and $\tilde{\mu}_B$ are the modified chemical potentials of components A and B, respectively. The diffusion rates of components A and B in the solution are described by the diffusion constants D_A and D_B, respectively. Note that the solvent S is considered implicitly, whose evaporation is described by

$$\frac{dh}{dt} = v_e \phi_S^* \quad (4)$$

where h is the thickness of the liquid film, ϕ_S^* is the volume fraction of component S at the surface of the liquid film, and v_e is the evaporation rate of the solvent. More details are given in the Supporting Information.

The simulation results of J71:ITTC in CB solution are plotted in **Figure 4**a (t = 0–110) and 4b (t = 155). At the beginning of solvent evaporation (t = 1), the surface mesophase appears, and the depleted sublayer is also observed in the plots. As time advances (t = 1–50), the surface segregation becomes more pronounced while the component ratio underneath the depleted sublayer in the liquid film remains the same. After most of the CB solvent evaporated (t > 80), the component distributions for J71 and ITTC turn to be bilayer and then gradually evolve into composition waves. Finally (t = 155, Figure 4b), the solvent is completely evaporated as the simulated film thickness and mean component ratio no longer vary with the reduced time (Figure S12, Supporting Information). The period of such simulation wave is 2T for the thin film deposited from CB. A_m value is 0.32, which is consistent with the experimental data in Figure 3g. For CF solution, as shown in Figure 4c (t = 0–22) and Figure 4d (t = 24.4), a similar evolution is observed. Due to the low boiling point of CF, the whole evaporation time is shorter than that of the CB solution (Figure S12, Supporting Information), which leads to 2.5 periods of "wave" and a smaller A_m value of 0.09 compared with that of CB solution. It needs to be noted that the orange arrow in Figure 4a,c indicates increasing simulation time, which is scaled by the characteristic time (Numerical Methods in the Supporting Information), and R_g serves as a reference length to scale all relevant length coordinates presented in Figure 4. As for Figure 4a,c, the far left of the diagram represents the bottom of the liquid film, while the surface of the liquid film is in the far right of diagram. The 0 R_g in Figure 4b,d has the same coordinate significance in

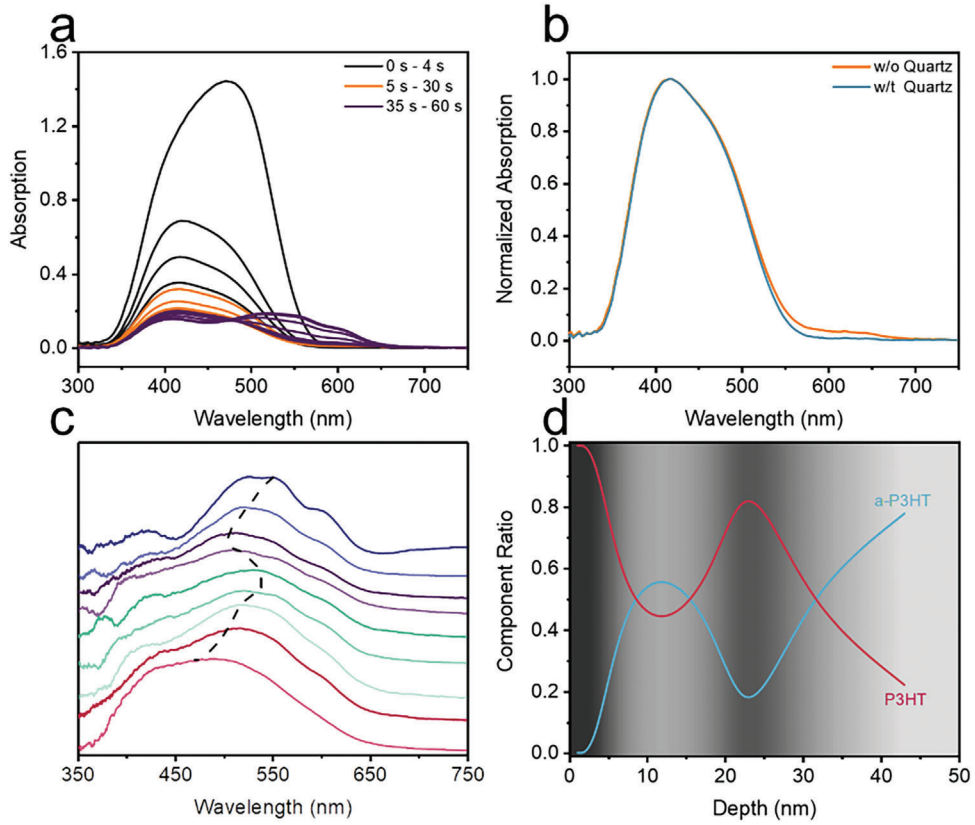

Figure 5. The composition wave phase evolution in (quasi-) neat semicrystalline polymer films. Single-component neat semicrystalline polymer is usually composed of both crystalline and amorphous microdomains. For clarity, here the crystalline conjugated polymer regioregular rr-P3HT blended with its isomer regiorandom rra-P3HT are studied as a model quasi-single-component P3HT system. a) Time-dependent absorption spectra of rr-P3HT:rra-P3HT (1:1) spin-coated from its *o*-DCB solution. The appearance of absorption peak at 610 nm during solvent evaporation implies the formation of surface mesophase at the air-solvent interface. b) The normalized absorption spectra of rr-P3HT:rra-P3HT solution during solvent evaporation with and without quartz covering the wet solution film. Without quartz, the absorption peak at 610 nm indicates the formation of surface mesophase. c) FLAS of rr-P3HT:rra-P3HT films, and the dashed curve shows the oscillation of composition varying with film-depth position, indicating a composition wave. The dash line shows the main peak shift of rr-P3HT in blend thin film, indicating the composition variation along the film-depth direction. d) Composition distribution profiles along the film-depth direction as numerically extracted from (c). The alternative grayscale area shows the phase of the composition wave.

Figure 3g, meaning the surface of dry films. Moreover, conditions of different initial volume fractions of J71 and ITTC (6:4 and 4:6) are also applied in simulations, as shown in Figure S12g,h (Supporting Information), and the results are also well-matched with the experimental data.

These simulations reveal that the Peclet number, $P_e = v_e R_g / D_A$, the initial volume fractions of solutes, the initial film thickness, and the confinement of the organic thin film are all important for determining the evolution kinetics and the wave pattern of the drying thin films in the film-depth direction. At the beginning, the thickness of organic liquid film decreases as the solvents gradually evaporate. Then, the phase transition occurs only after the concentration of the solutes enters the two-phase region. In this scenario, the film thickness may reduce to a value that can only allow development of a special pattern for composition wave. Thus, such a simulation can be a valuable tool to aid the design of the structure of organic thin films, such as facilitating the choice of solvents, initial processing conditions, etc. in replacement of lengthy and costly experimental explorations.

2.4. Composition Wave Evolution in (Quasi-) Neat Semicrystalline Polymer Films

To explore whether such wave-like propagation of phase evolution only occurs in multicomponent systems with very contrasting molecular structure (polymer and small molecule), an isomer system comprising rr-P3HT (forms semicrystalline films) and rra-P3HT (forms amorphous films) is investigated. For clarity, here the rr-P3HT:rra-P3HT films are studied as a model quasi-single-component P3HT system. Time-dependent absorption spectroscopy is utilized to investigate the phase evolution dynamics for rr-P3HT:rra-P3HT blend solution, and the overall experimental process is shown in **Figure 5**a. At the initial stage after starting spin-coating (0–4 s, black lines), a broad absorption peak occurs between 350 and 600 nm, and its intensity gradually becomes weaker as a large fraction of the blend solution is removed during spin-coating. Subsequently, a new peak at 610 nm, which is assigned to the pre–aggregated rr-P3HT, suddenly protrudes and keeps constant for nearly 30 s during which the main peak intensity slightly decreases as solvent evaporates. To

confirm whether the pre–aggregation of rr-P3HT appears within the blend solution or at the interface, a quartz plate was placed on top of blend solution of rr-P3HT:rra-P3HT to prevent *o*-DCB evaporation (Figure 5b). This leads to the vanishing of the pre–aggregated peak at 610 nm, making it clear that the pre–aggregation occurs at the air-solvent interface. Also note the presence of the peak of rra-P3HT consistently situates at 408 nm during the entire evaporation process. Moreover, our previous work[42] demonstrated a double-layer morphology of P3HT:PS (amorphous polystyrene) with ultrathin P3HT (thickness about 1–2 nm) on the top surface of P3HT:PS blend films, which may be induced by the surface mesophase of P3HT in such multicomponent system. Additional FLAS of rr-P3HT:rra-P3HT film is performed with the data shown in Figure 5c. The dash line labels the main peak shift of rr-P3HT, demonstrating the high contents of rr-P3HT tend to present red-shift of main peak in its corresponding sublayer spectrum, thereby indicating composition wave exists in such isomer system. Subsequent composition calculation in Figure 5d also confirms the enrichment of rr-P3HT in the skin layer and another major part of rr-P3HT is concentrated at 20–30 nm below the surface. The periods of "composition wave" for rr-P3HT:rra-P3HT isomer system is 2T per 50 nm, and the A_m and A_s are 0.29 and 0.5 for such system, which is relatively large due to high boiling-point *o*-DCB. Besides, the velocity of such wave is smaller than that in J71:ITTC and is about 0.42 nm s^{-1} due to slower evaporation rate of *o*-DCB.

Hereto, we have made a thorough inquiry into composition wave of phase evolution dynamics initiated and propagated by surface mesophase in organic multicomponent solutions, leading to the wave-like phase segregation and highly varied component distribution along film-depth direction. Not only are the dynamic process and mechanism extensively appropriate for more than 80% of randomly examined solution-processed thin films for OPV cells composed of totally different semiconductors but also for isomer systems, demonstrating that the difference in crystallinity can also result in wave-like phase evolution dynamics even though the binary polymer system has exactly identical structural unit at the molecular level. In one word, the diversity of solubility, crystallinity and diffusion rate in the solution have a combined effect on the formation of composition wave in multicomponent systems, which enlighten us that such phenomenon may occur in a single component polymer system due to its polydispersity, including crystallinity and molecular weight.

By examining a large number of organic systems holding wave-like composition distribution properties in Table S2 (Supporting Information), it is found that the content of surface is mainly governed by donor/polymer. The low boiling point solvent is prone to more than 1T inner the films. The value of A_s is commonly far bigger than that of A_m, meaning the enrichment of donor/polymer and larger phase separation on the surface. For PM6:Y6 systems (Table S2, Supporting Information), high boiling point solvents, such as CB and *o*-DCB, makes "wave" possess larger A_s and A_m compared with CF, resulting in a large decrease in device performance. In addition, some other empirical conclusions are drawn as follows. As for such polymer:small-molecule systems, polymer aggregations on the surface for such blends film are very detrimental to the power conversion efficiency of regular devices, whereas inverted ones behave better tolerance to such surface aggregation. The evaporation rate of solvents also affects the amount of polymer on the surface, and high boiling point solvents often afford sufficient time for the kinetic evolution, which leads to more surface aggregation and phase separation along film depth direction. Overall, the high-efficient combinations generally have the better compatibility of the donor and acceptor in the development of organic solar cells, and low-boiling chloroform is preferred for researchers as long as the solubility for active materials is not compromised.

3. Conclusion

Organic thin films deposited from solution are widely used in optoelectronic devices. During solvent evaporation, the phase evolution of different components is not synchronic in terms of both time and space (film-depth) scales. In this work, a wave-like propagation of phase transition, namely a composition wave, is recognized, which has typical wave properties with wavelengths of 30–100 nm, amplitudes of 0.10–0.45, and velocity (0.1–20 nm s^{-1}). Such composition waves are seen in blends of components with dissimilar chemical structure like the mixture of the nonfullerene acceptor ITTC with the donor polymer J71, and even for a mixture of the semicrystalline polymer rr-P3HT with its amorphous isomer rra-P3HT. These wave properties are closely correlated with solvent evaporation rate and diffusion rates of organic molecules, which determines the transient composition gradient along the surface-normal direction. The results reveal that the anisotropic phase evolution dynamics at different locations within the still-wet films leads to the anisotropic film morphology. A surface mesophase initiates the propagation of composition waves toward the substrate. Simulated dynamics are in good agreement with the experimental results, demonstrating the widespread extensive existence of surface mesophase and composition waves in such multicomponent systems as used in the organic optoelectronics community. This work provides important novel insight into the morphology evolution of multicomponent organic thin films and enables advanced film manipulation in the future for superior performance in optoelectronic devices.

Supporting Information

Supporting Information is available from the Wiley Online Library or from the author.

Acknowledgements

J.Y. and Z.S. contributed equally to this work. This work was supported by the National Natural Science Foundation of China (grant Nos. 51873172, 21873021, 52273026, and 51907148) and the Key Scientific and Technological Innovation Team Project of Shaanxi Province (grant No. 2021GXLH-Z-055). G.L. supervised the project. All the authors wrote and reviewed the manuscript.

Conflict of Interest

The authors declare no conflict of interest.

Data Availability Statement

The data that support the findings of this study are available from the corresponding author upon reasonable request.

Keywords

organic electronic devices, organic thin films, surface mesophase, time- and space-resolved optical spectroscopies

Received: February 22, 2023
Revised: May 10, 2023
Published online: June 14, 2023

[1] E. Dauzon, X. Sallenave, C. Plesse, F. Goubard, A. Amassian, T. D. Anthopoulos, *Adv. Mater.* **2021**, *33*, 2101469.
[2] M. Ghasemi, N. Balar, Z. Peng, H. Hu, Y. Qin, T. Kim, J. J. Rech, M. Bidwell, W. Mask, I. McCulloch, W. You, A. Amassian, C. Risko, B. T. O'Connor, H. Ade, *Nat. Mater.* **2021**, *20*, 525.
[3] C. Han, J. Wang, S. Zhang, L. Chen, F. Bi, J. Wang, C. Yang, P. Wang, Y. Li, X. Bao, *Adv. Mater.* **2023**, *35*, 2208986.
[4] G. Lu, J. Blakesley, S. Himmelberger, P. Pingel, J. Frisch, I. Lieberwirth, I. Salzmann, M. Oehzelt, R. Di Pietro, A. Salleo, N. Koch, D. Neher, *Nat. Commun.* **2013**, *4*, 1588.
[5] Y. Wei, Z. Chen, G. Lu, N. Yu, C. Li, J. Gao, X. Gu, X. Hao, G. Lu, Z. Tang, J. Zhang, Z. Wei, X. Zhang, H. Huang, *Adv. Mater.* **2022**, *34*, 2204718.
[6] L. Zhang, L. Hu, X. Wang, H. Mao, L. Zeng, L. Tan, X. Zhuang, Y. Chen, *Adv. Funct. Mater.* **2022**, *32*, 2202103.
[7] X. Zhang, G. Li, S. Mukherjee, W. Huang, D. Zheng, L. W. Feng, Y. Chen, J. Wu, V. K. Sangwan, M. C. Hersam, D. M. DeLongchamp, J. Yu, A. Facchetti, T. J. Marks, *Adv. Energy Mater.* **2021**, *12*, 2102172.
[8] J. J. van Franeker, M. Turbiez, W. Li, M. M. Wienk, R. A. Janssen, *Nat. Commun.* **2015**, *6*, 6229.
[9] J. H. Lee, H. H. Choi, Y. D. Park, J. E. Anthony, J. A. Lim, J. Cho, D. S. Chung, J. Hwang, H. W. Jang, K. Cho, W. H. Lee, *Adv. Funct. Mater.* **2018**, *28*, 1802875.
[10] E. F. Manley, J. Strzalka, T. J. Fauvell, T. J. Marks, L. X. Chen, *Adv. Energy Mater.* **2018**, *8*, 1800611.
[11] Z. Bi, H. B. Naveed, Y. Mao, H. Yan, W. Ma, *Macromolecules* **2018**, *51*, 6682.
[12] Z. Peng, Y. Zhang, X. Sun, W. Zhao, F. Bian, Y. Geng, L. Ye, C. Yang, *Adv. Funct. Mater.* **2023**, *13*, 2213248.
[13] Q. Liang, X. Jiao, Y. Yan, Z. Xie, G. Lu, J. Liu, Y. Han, *Adv. Funct. Mater.* **2019**, *29*, 1807591.
[14] G. Qu, K. S. Park, P. Kafle, F. Zhang, J. J. Kwok, B. B. Patel, D.-M. Smilgies, L. Thomsen, C. R. McNeill, Y. Diao, *Chem. Mater.* **2020**, *32*, 6043.
[15] A. J. Pearson, T. Wang, A. D. F. Dunbar, H. Yi, D. C. Watters, D. M. Coles, P. A. Staniec, A. Iraqi, R. A. L. Jones, D. G. Lidzey, *Adv. Funct. Mater.* **2013**, *24*, 659.
[16] L. Ye, H. Hu, M. Ghasemi, T. Wang, B. A. Collins, J. H. Kim, K. Jiang, J. H. Carpenter, H. Li, Z. Li, T. McAfee, J. Zhao, X. Chen, J. L. Y. Lai, T. Ma, J. L. Bredas, H. Yan, H. Ade, *Nat. Mater.* **2018**, *17*, 253.
[17] Z. Wang, K. Gao, Y. Kan, M. Zhang, C. Qiu, L. Zhu, Z. Zhao, X. Peng, W. Feng, Z. Qian, X. Gu, A. K. Jen, B. Z. Tang, Y. Cao, Y. Zhang, F. Liu, *Nat. Commun.* **2021**, *12*, 332.
[18] Z. Liang, M. Li, Q. Wang, Y. Qin, S. J. Stuard, Z. Peng, Y. Deng, H. Ade, L. Ye, Y. Geng, *Joule* **2020**, *4*, 1278.
[19] A. Levitsky, S. A. Schneider, E. Rabkin, M. F. Toney, G. L. Frey, *Mater. Horiz.* **2021**, *8*, 1272.
[20] M. Ghasemi, H. Hu, Z. Peng, J. J. Rech, I. Angunawela, J. H. Carpenter, S. J. Stuard, A. Wadsworth, I. McCulloch, W. You, H. Ade, *Joule* **2019**, *3*, 1328.
[21] S. Marina, N. P. Kaufmann, A. Karki, E. Gutierrez-Meza, E. Gutierrez-Fernandez, J. Vollbrecht, E. Solano, B. Walker, J. H. Bannock, J. de Mello, C. Silva, T. Q. Nguyen, D. Cangialosi, N. Stingelin, J. Martin, *Adv. Mater.* **2020**, *32*, 2005241.
[22] Y. Vaynzof, D. Kabra, L. Zhao, L. L. Chua, U. Steiner, R. H. Friend, *ACS Nano* **2011**, *5*, 329.
[23] H. Yao, L. Ye, J. Hou, B. Jang, G. Han, Y. Cui, G. M. Su, C. Wang, B. Gao, R. Yu, H. Zhang, Y. Yi, H. Y. Woo, H. Ade, J. Hou, *Adv. Mater.* **2017**, *29*, 1700254.
[24] H. Bin, L. Gao, Z. G. Zhang, Y. Yang, Y. Zhang, C. Zhang, S. Chen, L. Xue, C. Yang, M. Xiao, Y. Li, *Nat. Commun.* **2016**, *7*, 13651.
[25] L. Perdigón-Toro, L. Q. Phuong, F. Eller, G. Freychet, E. Saglamkaya, J. I. Khan, Q. Wei, S. Zeiske, D. Kroh, S. Wedler, A. Köhler, A. Armin, F. Laquai, E. M. Herzig, Y. Zou, S. Shoaee, D. Neher, *Adv. Energy Mater.* **2022**, *12*, 2103422.
[26] F. Zhao, S. Dai, Y. Wu, Q. Zhang, J. Wang, L. Jiang, Q. Ling, Z. Wei, W. Ma, W. You, C. Wang, X. Zhan, *Adv. Mater.* **2017**, *29*, 1700144.
[27] R. Yu, S. Zhang, H. Yao, B. Guo, S. Li, H. Zhang, M. Zhang, J. Hou, *Adv. Mater.* **2017**, *29*, 1700437.
[28] H. Bin, Z. G. Zhang, L. Gao, S. Chen, L. Zhong, L. Xue, C. Yang, Y. Li, *J. Am. Chem. Soc.* **2016**, *138*, 4657.
[29] H. Zhang, H. Yao, J. Hou, J. Zhu, J. Zhang, W. Li, R. Yu, B. Gao, S. Zhang, J. Hou, *Adv. Mater.* **2018**, *30*, 1800613.
[30] W. Zhao, D. Qian, S. Zhang, S. Li, O. Inganas, F. Gao, J. Hou, *Adv. Mater.* **2016**, *28*, 4734.
[31] J. Wang, J. Zhang, Y. Xiao, T. Xiao, R. Zhu, C. Yan, Y. Fu, G. Lu, X. Lu, S. R. Marder, X. Zhan, *J. Am. Chem. Soc.* **2018**, *140*, 9140.
[32] R. Sun, Y. Wu, J. Guo, Y. Wang, F. Qin, B. Shen, D. Li, T. Wang, Y. Li, Y. Zhou, G. Lu, Y. Li, J. Min, *Energy Environ. Sci.* **2021**, *14*, 3174.
[33] Z. Xu, L.-M. Chen, G. Yang, C.-H. Huang, J. Hou, Y. Wu, G. Li, C.-S. Hsu, Y. Yang, *Adv. Funct. Mater.* **2009**, *19*, 1227.
[34] Y. Yan, X. Liu, T. Wang, *Adv. Mater.* **2017**, *29*, 1601674.
[35] L. Huang, G. Wang, W. Zhou, B. Fu, X. Cheng, L. Zhang, Z. Yuan, S. Xiong, L. Zhang, Y. Xie, A. Zhang, Y. Zhang, W. Ma, W. Li, Y. Zhou, E. Reichmanis, Y. Chen, *ACS Nano* **2018**, *12*, 4440.
[36] Q. Li, L. M. Wang, S. Liu, X. Zhan, T. Zhu, Z. Cao, H. Lai, J. Zhao, Y. Cai, W. Xie, F. Huang, *ACS Appl. Mater. Interfaces* **2019**, *11*, 45979.
[37] A. Tada, Y. Geng, Q. Wei, K. Hashimoto, K. Tajima, *Nat. Mater.* **2011**, *10*, 450.
[38] J. Ma, K. Hashimoto, T. Koganezawa, K. Tajima, *J. Am. Chem. Soc.* **2013**, *135*, 9644.
[39] F. Wang, K. Hashimoto, K. Tajima, *Adv. Mater.* **2015**, *27*, 6014.
[40] L. Zhang, N. Yi, W. Zhou, Z. Yu, F. Liu, Y. Chen, *Adv. Sci.* **2019**, *6*, 1900565.
[41] T. Okuzono, K. Ozawa, M. Doi, *Phys. Rev. Lett.* **2006**, *97*, 136103.
[42] Y. Hu, P. Wei, X. Wang, L. Bu, G. Lu, *Phys. Rev. Appl.* **2018**, *10*, 054024.